JGR Solid Earth

RESEARCH ARTICLE
10.1029/2020JB020416

Key Points:
- We analyzed H_2O contents in cpx, opx, and garnet in Proterozoic lower crustal xenoliths from Colorado
- Mineral H_2O content was used to reconstruct bulk rock and calculate melt H_2O
- Xenoliths represent metamorphosed igneous cumulates from high-P, hydrous magmas

Supporting Information:
- Supporting Information S1
- Table S1
- Table S2

Correspondence to:
E. J. Chin,
e8chin@ucsd.edu

Citation:
Chin, E. J., Curran, S. T., & Farmer, G. L. (2020). Squeezing water from a stone: H_2O in nominally anhydrous minerals from granulite xenoliths and deep, hydrous fractional crystallization. *Journal of Geophysical Research: Solid Earth*, *125*, e2020JB020416. https://doi.org/10.1029/2020JB020416

Received 17 JUN 2020
Accepted 2 SEP 2020
Accepted article online 14 SEP 2020

Squeezing Water From a Stone: H_2O In Nominally Anhydrous Minerals From Granulite Xenoliths and Deep, Hydrous Fractional Crystallization

Emily J. Chin[1], Sean T. Curran[1], and G. Lang Farmer[2]

[1]Geosciences Research Division, Scripps Institution of Oceanography, University of California, San Diego, La Jolla, CA, USA, [2]Department of Geological Sciences and CIRES, University of Colorado Boulder, Boulder, CO, USA

Abstract Water is key to plate tectonics on Earth, which, in turn, is vital to the production of continental crust. Although arc lavas erupt in a volatile-rich state and calc-alkaline arc plutons are distinguished by the presence of hydrous minerals such as hornblende and biotite, the water content of arc magmas earlier in their evolution—in the deep crust—remains poorly constrained. Here, we report H_2O contents in nominally anhydrous minerals measured in situ on petrographic thin sections by secondary ion mass spectrometry of Proterozoic deep crustal xenoliths from Colorado, USA. Clinopyroxene, orthopyroxene, and garnet contain average H_2O contents ranging from 75–760, 233–410, and 42–139 ppm, respectively. Reconstructed bulk rock H_2O contents range from ~60 to ~650 ppm. Intermineral H_2O ratios overlap experimental mineral/melt *D* values and are used to calculate H_2O of melts last in equilibrium with the xenoliths. We propose that these xenoliths represent cumulates fractionated from a primitive, hydrous (≥1 wt.% H_2O) melt at high (~1 GPa) pressures, similar to conditions in modern subduction zones and potentially associated with widespread arc accretion that formed the core of North America in the Precambrian.

1. Introduction

Since ~3 Ga, global subduction has played an important role in generating extensive calc-alkaline rocks associated with continental crust (Arndt, 2013). Two distinct mafic, igneous protoliths exist in the lower arc crust. The first is eclogite in a strict sense, a metamorphic rock derived from tholeiitic basalt of subducting oceanic crust (Defant & Drummond, 1990), terranes of oceanic affinity (Cavosie & Selverstone, 2003; Scholl et al., 1986), or accreted mafic underplates of oceanic plateaus (Condie, 1999). The second is arclogite (Lee & Anderson, 2015)—defined as a pyroxene and garnet-rich cumulate derived from deep crustal igneous fractionation of primitive, hydrous basaltic arc magmas (Ducea, 2002; Lee, 2014). Owing to their mafic compositions, partial melting of both eclogite and arclogite will yield silica-rich melts, making them appropriate candidates for generating continental crust. Silica-rich, buoyant arc crust can also be left behind if dense mafic lower crust physically founders back into the mantle. How much of the continental crust over Earth's history was derived from remelting preexisting eclogite (Rapp et al., 2003) versus de novo arclogite fractionation (Jagoutz, 2010; Lee et al., 2006) remains an ongoing question.

Magmatic water content is central to this debate, because water content of primary magmas is an important discriminator for tholeiitic versus calc-alkaline settings (Sobolev & Chaussidon, 1996). Eclogitic protoliths should be water-poor owing to prograde metamorphism and dehydration; melts in equilibrium with such protoliths would reflect these anhydrous conditions. By contrast, high-temperature igneous arclogites should, in theory, reflect equilibrium with hydrous melts because primitive calc-alkaline magmas already contain at least ~2 wt.% H_2O (Plank et al., 2013). Subsequent fractional crystallization evolves more hydrous derivative melts that have been shown to fractionate garnet and clinopyroxene-rich cumulates in the lower crust (Lee et al., 2006; Muntener & Ulmer, 2006) and amphibole-rich cumulates in the middle crust (Davidson et al., 2007). The budget of magmatic water in the deep crust has profound consequences for cumulate mineralogy, lower crustal rheology, and ultimately bulk crustal composition. For instance, high magmatic water expands the liquidus field of pyroxene over plagioclase (Kushiro & Yoder, 1969), resulting in pyroxenite cumulates dominating arc lower crust, compared to plagioclase-rich cumulates in oceanic lower crust (Chin et al., 2018). Water also plays an important role in crusting melting (Collins et

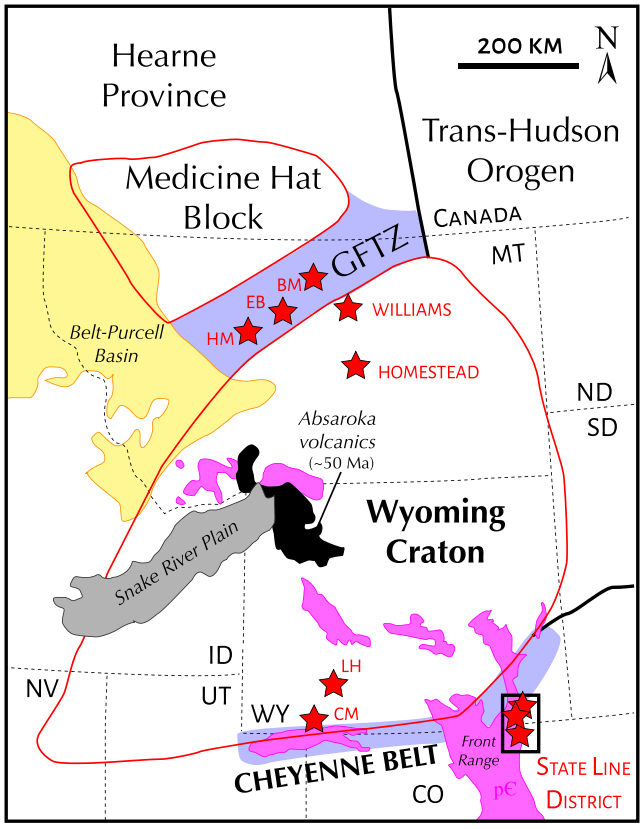

Figure 1. Geologic and tectonic setting. Simplified map of the Wyoming Province showing key geologic features. Xenolith localities are denoted by red stars: BM = Bearpaw Mountains, EB = Eagle Butte, HM = Highwood Mountains, CM = Cedar Mountain, LH = Leucite Hills. GFTZ = Great Falls tectonic zone.

al., 2020). Even at ppm levels, water in mineral lattices can significantly enhance crystal plasticity and decrease rock viscosity (Hirth & Kohlstedt, 1995) that, combined with the pyroxene and garnet-rich nature of lower crustal arc rocks, may promote deformation and destabilization of dense, mafic arc crust and survival of buoyant, felsic continental crust.

Determining the water content of a primary magma is challenging because such magmas are rarely, if ever, directly sampled. However, early-formed phenocrysts or cumulates, if not subject to later rehydration or dehydration, could "lock" in the water content of the melt last in equilibrium with the crystal. Here, we use this approach to probe both the hydration state of stable lower continental crust and to infer the water content of magmas that fractionated this crust. We report water contents, measured by secondary ion mass spectrometry, in nominally anhydrous minerals (NAMs) in granulite xenoliths from the Devonian-age State Line Kimberlite District, northern Colorado, USA. Our samples are ideal for constraining the water content of stable continental lower crust because they record Paleoproterozoic crustal formation ages and, importantly, erupted well before the Cenozoic Laramide Orogeny, which is thought to have caused a widespread hydrous overprint of the deep lithosphere beneath southwestern North America (Jones et al., 2015; Li et al., 2008). An evaluation of previously published bulk rock major element data, combined with new clinopyroxene major element data and our new H_2O contents in NAMs, suggests that the State Line xenoliths could represent deep crustal cumulates, rather than restites or crystallized basaltic melts. We go a step further and propose that the melt that crystallized the protoliths of the State Line xenoliths was hydrous (≥1 wt.% H_2O), based on calculated H_2O contents of liquids last in equilibrium with the xenoliths. A plausible scenario for such a melt could have been subduction magmatism associated with the Yavapai arc terrane, one of several Proterozoic arc building blocks of the North American continent.

2. Geologic Setting and Previous Work

2.1. Geologic Background

The State Line Kimberlite District comprises ~100 kimberlite diatremes of Devonian age, a large number of which bear mantle and lower crustal xenoliths (Eggler et al., 1987). The diatremes were emplaced within Proterozoic continental crust of the Colorado Province (Bickford et al., 1986), just south of the boundary with Archean crust of the Wyoming Craton (Figure 1). The Wyoming Craton and Medicine Hat Block represent part of a number of Archean cratonic cores amalgamated in the Paleoproterozoic to form the nucleus of Laurentia (Whitmeyer & Karlstrom, 2007). Starting at ~1.8 Ga, a series of oceanic terranes and island arcs accreted to the southern edge of the Wyoming Craton. These accreted arc terranes form large-scale, northeast trending belts with juvenile crust ages decreasing away from the cratonic core (Whitmeyer & Karlstrom, 2007): the Yavapai Province (1.7–1.8 Ga), the Mazatzal Province (1.7–1.6 Ga), and the Granite-Rhyolite Province (1.55–1.35 Ga). The core of the North American continent coalesced completely by ~1.0 Ga (the Grenville Orogeny).

The Colorado Province remained quiescent until the end of the Paleozoic, when regional deformation developed the Ancestral Rocky Mountains. The next major tectonic event to impact the Colorado Province did not occur until ~70 Ma with the Laramide Orogeny, classically attributed to low-angle subduction of the Farallon Plate beneath Western North America (Dickinson & Snyder, 1978). Low-angle subduction induced significant fluid metasomatism and hydration of the deep lithosphere across much of the western United States (Humphreys et al., 2003). The impact of deep lithospheric hydrous metasomatism is manifested by amphibole and biotite-rich lower crustal xenoliths erupted in 3.0 to 0.89 Ma lamproites (Lange

et al., 2000) to the northwest of the Devonian-age State Line kimberlites (Leucite Hills; Figure 1), as well as distinctive geochemical signatures in Cenozoic volcanic rocks throughout the southwestern United States ascribed to melting of hydrous metasomatized continental lithosphere (Farmer et al., 2020). Importantly, the xenoliths from the State Line kimberlites do not show evidence for hydrous metasomatism (Farmer et al., 2005), and their Devonian eruption ages means they were never impacted by the hydrous overprint of the Laramide Orogeny. Thus, the State Line lower crustal xenoliths represent a potentially pristine glimpse of the water content of lower continental crust preserved since its formation.

2.2. Lower Crustal Xenoliths

Lower crustal xenoliths from the State Line District include a variety of mafic lithologies but are dominated by (nominally anhydrous) mafic granulites, with subordinate amphibolites, anorthosites, and gabbroic xenoliths (Bradley & McCallum, 1984; Farmer et al., 2005). We selected nine samples (Table 1) from the Sloan 2 (SD2), Nix (NX4), and Schaeffer (SH) kimberlite pipes located in the Front Range in north central Colorado (Bradley & McCallum, 1984). Some of these xenoliths were previously analyzed for whole-rock, mineral compositions, Sr-Nd isotopes, and U-Pb zircon ages (Farmer et al., 2005). Within the mafic granulites, Bradley and McCallum (1984) defined three groups: two pyroxene granulites, two pyroxene garnet granulites, and clinopyroxene garnet granulites. The final equilibration conditions of garnet-bearing granulites range from ~1–1.5 GPa and ~700–800°C (Farmer et al., 2005). In addition, xenoliths of mantle eclogite are common (Ater et al., 1984). Although most of these eclogitic xenoliths are eclogites in a strict sense (e.g., largely bimineralic rocks containing >75% garnet and omphacitic clinopyroxene), a small number of xenoliths were also classified as "eclogite" by Farmer et al. (2005) (e.g., sample SH-E1), but as we discuss later in this paper, some of these previously classified eclogites do not resemble mid-ocean ridge basalts (MORB)-eclogites in a strict sense. Generally speaking, garnet-bearing granulites are compositionally gradational to eclogites (Ater et al., 1984; Bradley & McCallum, 1984). For example, Bradley and McCallum (1984) noted that the mafic garnet-clinopyroxene granulites have relatively high jadeite content in their clinopyroxenes, similar to the sodic clinopyroxenes in the eclogite xenoliths, suggesting a gradual transition into eclogite facies. Here, we will refer to the aforementioned three groups of nominally anhydrous mafic granulites collectively as "lower crustal xenoliths" and divide them into two broad groups based on mineralogy: garnet-free and garnet-bearing. No "true" eclogites from Ater et al. (1984), nor amphibolites, are examined in this paper.

The modal mineralogy of the State Line lower crustal xenoliths is dominated by clinopyroxene, orthopyroxene, plagioclase, and garnet; these phases constitute >90% by volume of most of the xenoliths (Bradley & McCallum, 1984). Amphibole is present in some 2-pyroxene granulites (Bradley & McCallum, 1984; Farmer et al., 2005) but is absent or rare in garnet-bearing xenoliths. The most common accessory minerals are ilmenite, rutile, and apatite. Farmer et al. (2005) also reported minor amounts of zircon, barite, and K-feldspar. The latter two minerals were interpreted as grain boundary contaminants from the host kimberlite, as observed in K-rich phases along grain boundaries and K-feldspar occasionally replacing plagioclase grains.

U-Pb ages of zircons from State Line lower crustal xenoliths show a wide range of dates, with a dominant population of $^{207}Pb/^{206}Pb$ dates of 1.73 to 1.6 Ga (Farmer et al., 2005). This age population overlaps the Yavapai Orogeny (1.71–1.68; Whitmeyer & Karlstrom, 2007). There are also smaller populations of zircons with Archean ages (presumably inherited and only present in amphibolites), ~1.4 Ga ages, as well as dates coeval with the kimberlite eruption (Farmer et al., 2005). Unsurprisingly, zircons are rare in the more mafic xenoliths (e.g., the garnet-bearing, two-pyroxene lithologies). The oldest ages recorded by zircons in the mafic xenoliths are ~1.72 Ga, with evidence of overprinting (deduced from sector zoning; Farmer et al., 2005). In summary, Farmer et al. (2005) interpreted the U-Pb age systematics of the State Line xenoliths to largely reflect lower crustal growth during the Paleoproterozoic, with metamorphic zircon overgrowths occurring at 1.3–1.4 Ga, coeval with the widespread regional metamorphic event at that time in North America.

3. Materials and Methods

3.1. Secondary Ion Mass Spectrometry

We analyzed H_2O by ion microprobe in nominally anhydrous minerals in situ in petrographic thin sections. New one-inch round thin sections were made from previously collected xenolith material. Prior to thin

Journal of Geophysical Research: Solid Earth

10.1029/2020JB020416

Table 1
Xenolith Descriptions, Petrography, and Modal Mineralogy

Sample ID	Rock type	Petrographic notes	Mineral modes
2-pyroxene granulites			
SD2-LC75	2-px granulite[a]	Medium-grained subhedral granoblastic	[26% cpx, 16% opx, 56% plag, trace oxides][b]
SD2-LC118	2-px granulite[a]	Medium-grained subhedral granoblastic; very similar texturally and mineralogically to SD2-LC75	
NX4-LC2	2-px granulite[a]	Medium-grained subhedral granoblastic	
2-pyroxene garnet granulites			
SD2-LC120	2-px gt granulite[a]	Medium- to coarse-grained anhedral granoblastic orthopyroxene and plagioclase, with interstitial clinopyroxene and ilmenite and rutile. Garnet occurs throughout in fine-grained clusters (resembling foam), as well as in weakly developed coronas around orthopyroxene. Rutile grains are subrounded and medium grained.	[35% plag, 30% opx, 25% gt, 10% cpx, minor ilmenite and K-feldspar, trace rutile and zircon][c]
SD2-LC71	2-px gt granulite[a]	Medium- to coarse-grained anhedral granoblastic Plagioclase contains deformation twins Garnet and clinopyroxene show a coarse myrmekitic texture organized into loosely defined coronas	[35% cpx, 12% opx, 29% gt, 23% plag, trace oxides][b]
NX4-LC1	2-px gt granulite[a]	Medium-grained subhedral granoblastic Weak foliation defined by alignment of elongated opx, cpx, ilmenite[a] Ilmenites are widely distributed; garnet coronas appear to have nucleated predominantly on ilmenite grains Plagioclase contains deformation twins	
Opx-free garnet granulite			
SD2-LC74	Cpx-gt granulite[a]	Medium- to coarse-grained subhedral granoblastic Garnet shows various textures, from fine-grained, foamy clusters (symplectites) to coarse grains near ilmenite and clinopyroxene	[30% cpx, 30% gt, 35% plag, 3% ilm, minor K-feldspar, trace apatite, rutile, zircon, barite][c]
Xenoliths with <5% plagioclase			
SH-E1	Eclogite[a]	Nearly bimineralic, very coarse grained Large, round rutile grains dispersed throughout	[50% cpx, 48% gt, 2% rutile][d]
SD2-L110	2-px gt granulite	Resembles bimineralic granulites/eclogites petrographically Medium-grained subhedral granoblastic, weakly foliated with foliation defined by pyroxene or garnet-rich bands; some bands composed almost exclusively of coarse-grained clinopyroxene Plagioclase occurs interstitially between garnet and pyroxene Garnet-cpx coronas are either very small and fine-grained or absent	[40% cpx, 15% opx, 40% gt, 1% apatite, 3% plag, 1% phlogopite, trace oxide][d]

Note. Medium grained = 1 to 5 mm; coarse grained = >5 mm.
[a]Rock names for xenoliths are from Bradley (1985). [b]Calculated using least squares inversion of the whole-rock composition, if available (from Farmer et al., 2005) and average mineral compositions. [c]From Farmer et al., 2005. [d]Determined by pixel counting of whole thin section SEM EDS maps in Adobe Photoshop.

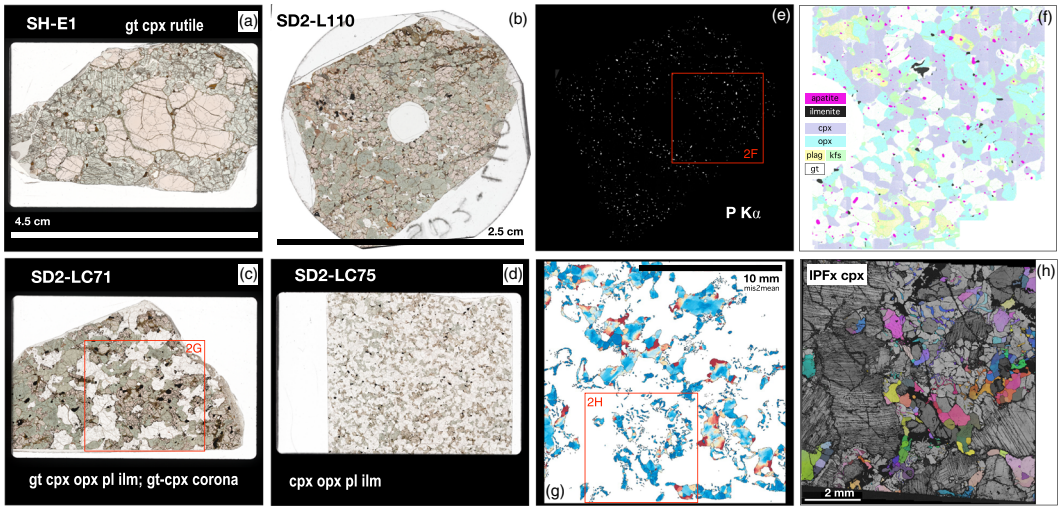

Figure 2. Representative petrographic and microtextural features of the State Line lower crustal xenoliths. (a–d) Plane-polarized light scans of thin sections. (b) Shows an example of a 1-inch round thin section with Suprasil glass mounted in the center for SIMS analyses (standard size thin sections are shown for other xenoliths because more area is available for observation). (a–h) Microbeam maps of SD2-L110 and SD2-LC71. (e) Is an EDS map of P highlighting the widespread distribution of apatite in xenolith SD2-L110. (f) Shows a false-color stacked EDS map of a subarea of e. (g) Is a mis2mean map of clinopyroxene grains from the red outlined area in (c). (h) Is the same area in (g) mapped by EBSD (shown here is an inverse pole figure map of clinopyroxene, superimposed on band contrast, in the x sample direction). Note abundance of deformation twins in plagioclase, as well as the similarity in IPF colors of within-corona, fine-grained clinopyroxene but more random colors in coarser-grained clinopyroxene.

section preparation, each billet was microdrilled and a grain of commercially available Suprasil glass (H_2O content 1 ppm; certified by Heraeus Quarzglas) was embedded in a central area of the xenolith (Figure 2b), ensuring a completely flat and well-polished surface. The purpose of the Suprasil is to monitor the instrumental H_2O background, a critical factor due to the ubiquitous presence of volatile-rich epoxy in petrographic thin sections and the typically low H_2O concentrations of nominally anhydrous minerals.

To minimize the background, prior to analysis the ion microprobe was baked for ~2 days to attain ultrahigh vacuum of $\sim 2 \times 10^{-10}$ torr. During a session, four thin sections, plus a separate block with mineral standards, were simultaneously introduced into the airlock at $\sim 5 \times 10^{-9}$ torr for at least 4 days, and in some cases up to 7 days, to ensure complete degassing of extraneous H_2O. Analyses were obtained using a CAMECA 7f-Geo SIMS, with the following operating parameters: primary Cs^+ beam with current of 4.5–5 nA, accelerating voltage of 10 kV, rastered over a 20 × 20 μm area with a field aperture limiting the secondary ion collection area to an 8 μm spot in the center of the rastered area. Each analysis comprised 2 min of presputtering then 30 cycles through the mass sequence ^{12}C, $^{16}O^1H$, ^{18}O, ^{19}F, ^{27}Al, Cl, and ^{30}Si. OH (or H_2O) was determined by using a mass resolving power of ~5,200 to separate $^{16}O^1H$ from ^{17}O; H_2O concentrations were determined using calibration curves (supporting information [SI] Figures S1–S6) developed using mineral standards from Aubaud et al. (2007), Mosenfelder et al. (2011), and Mosenfelder and Rossman (2013a, 2013b). During analyses, the ion image and counts were monitored at all times, and any visible "hot spots" in the ion image (presumably corresponding to tiny, hydrous inclusions or cracks) were noted and corresponding cycles deleted if necessary. ^{12}C was used as a monitor for contamination and/or cracks. Any measurements with high levels of ^{12}C, ^{19}F, or visible perturbations in the ion image were not reported.

Owing to the wide range of Si in minerals analyzed (garnet, pyroxene, plagioclase, amphibole, apatite, and phlogopite), in order to minimize matrix effects we normalized masses to ^{18}O, since the O contents of most silicate minerals are very similar (in contrast to Si which can vary by tens of weight %). Estimation of uncertainties followed the protocol outlined in Chin et al. (2016) and ranged from 10% to 15% (2 relative standard error [RSE]). Over the course of two analytical sessions, the average H_2O background ranged between ~15 and ~30 ppm; we background corrected all analyses using an average value of 23 ppm.

3.2. Electron Microprobe Analysis

Major element composition of pyroxenes, garnet, plagioclase, amphibole, and phlogopite were analyzed by electron microprobe using a CAMECA SX100 at Brown University (accelerating voltage 15 kV, beam current 20 nA, spot size 1 μm). In-house mineral standards and secondary mineral standards were used for calibration. Relative standard deviation was <1% for major elements and ~5% for minor elements.

3.3. EDS Mapping

Energy dispersive spectroscopy (EDS) maps were obtained for selected thin sections using an FEI Apreo LoVac field emission gun scanning electron microscope (SEM) at UC San Diego. Operating parameters were an accelerating voltage of 20 kV, beam current of 3.2 nA, and 250 μs dwell time.

3.4. EBSD

Electron backscatter diffraction (EBSD) maps of selected thin sections were obtained with an Oxford Instruments Symmetry EBSD detector on an FEI Apreo LoVac field emission gun (SEM) at UC San Diego. Thin sections were not carbon-coated prior to analysis, and maps were run in low vacuum mode. Automated EBSD maps were obtained using a step size of 5 μm, working distance between 26 and 28 mm, and accelerating voltage of 20 kV. Raw EBSD data were first cleaned using Oxford HKL CHANNEL5 software by removing wild spikes, followed by filling of nonindexed pixels down to five nearest neighbor pixels. Typically, cleaning was minimal as most indexing rates were 90% or higher. The cleaned EBSD data were then processed in the open source MTEX software to produce various types of crystal orientation maps (inverse pole figure [IPF], mis2mean, GOS) and pole figures.

4. Data and Results

4.1. Mineralogy and Petrography

Although previous studies (Bradley, 1985; Bradley & McCallum, 1984; Farmer et al., 2005) reported three distinct mineral assemblages in the State Line lower crustal xenolith suite, here we will broadly describe the xenoliths as two groups: garnet-free and garnet-bearing (Table 1). Garnet-free (i.e., two-pyroxene granulite) xenoliths are characterized by equigranular texture and numerous grains meeting at 120° triple junctions, exemplified in SD2-LC75 (Figure 2d). Mineral modes are dominated by plagioclase (~70%), with subequal amounts of clinopyroxene and orthopyroxene (~25–30% total pyroxene), and ~3–5% ilmenite. In contrast, garnet-bearing xenoliths vary widely in mineral modes and textures (Figure 2). Many garnet-bearing xenoliths have garnet-clinopyroxene coronas formed around ilmenite and plagioclase (Farmer et al., 2005). Below, we highlight notable features of three garnet-bearing xenoliths that encompass the mineralogical and textural complexity of the lower crustal xenolith suite.

SH-E1 (Figure 2a) (classified as an eclogite by Farmer et al., 2005) is very coarse grained (>1 cm) and composed of approximately equal amounts of clinopyroxene and garnet, with ~2% rutile. Clinopyroxene grains are often bent and deformed. Rutile occurs as 0.15 to 1.5 mm grains with various morphologies ranging from euhedral to rounded. Garnet occurs as very large (1–3 cm) grains with irregular, interlobate grain boundaries with clinopyroxene-occupied embayments.

SD2-L110 (Figure 2b) contains 40% clinopyroxene, 40% garnet, 15% orthopyroxene, 5% plagioclase + K-feldspar, ~1% apatite, and minor ilmenite, phlogopite, and hornblende. Clinopyroxene occasionally forms coarse-grained, equant bands (Figure 2b). Apatite is dispersed widely throughout the xenolith but is less abundant in clinopyroxene-rich bands (Figures 2e and 2f). Garnet-clinopyroxene coronas are uncommon and small in size.

SD2-LC71 contains 23% plagiocase, 35% clinopyroxene, 12% opx, 29% garnet, minor ilmenite, and trace amounts of K-feldspar. A distinctive feature of SD2-LC71 is the widespread occurrence of garnet-clinopyroxene coronas (Figures 2g and 2h), which may comprise up to 30% or more of the xenolith. Farmer et al. (2005) noted the abundance of garnet-clinopyroxene coronas in several State Line granulite xenoliths and interpreted the coronas to form from precursor orthopyroxene and calcic plagioclase. The coronas are irregular and lack concentric, mineral-specific zoning often seen in typical granulites (McLelland & Whitney, 1980). Within coronas, clinopyroxene occurs as small, worm-like grains surrounded

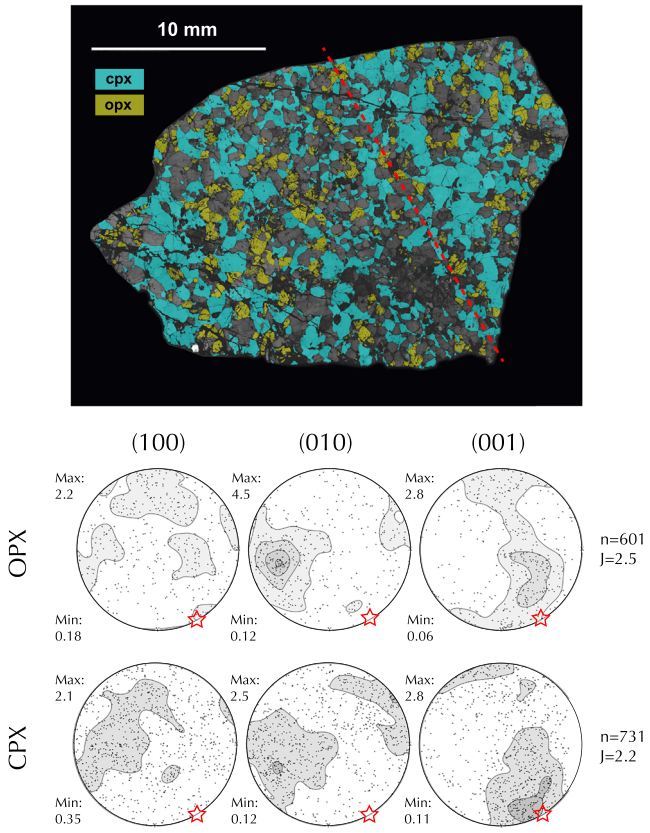

Figure 3. (top) Large-area EBSD map of SD2-L110. Only clinopyroxene and orthopyroxene are highlighted on top of band contrast. Dashed red line represents trace of foliation plane. (bottom) Pole figures (one point per grain) of orthopyroxene and clinopyroxene. n = number of grains, $J = J$ index, a measure of the CPO strength.

by garnet (Figures 2g and 2h); outside coronas, clinopyroxene occurs either as rims around orthopyroxene or as large porphyroclasts (Figure 2c).

In summary, the State Line garnet-free and garnet-bearing lower crustal xenoliths constitute a relatively simple mafic mineralogy, comprising two pyroxenes, plagioclase, ilmenite, and/or garnet. Olivine is absent. Garnet-bearing xenoliths show a greater diversity of textures and deformation microstructures compared to the garnet-free group. Some of these features, such as garnet-clinopyroxene coronas, attest to textural disequilibrium (Bradley & McCallum, 1984).

4.2. Deformation Microstructures

Microstructures of two xenoliths, SD2-L110 and SD2-LC71, were investigated in detail using EBSD mapping. In SD2-L110, clinopyroxene and orthopyroxene define a foliation (Figure 3) and exhibit measurable, but weak, crystallographic preferred orientations (CPOs) (Figure 3). The CPOs of both clinopyroxene and orthopyroxene are similar: Though weak, they show [001] maxima parallel to and [010] maxima perpendicular to the apparent lineation/trace of foliation (Figure 3). Such CPOs suggest slip along [001] and (010) as glide plane, consistent with naturally deformed deep lithospheric enstatites (Avé Lallemant, 1969).

A similar macroscopic foliation, loosely defined by garnet and clinopyroxene, is also observed in SD2-LC71 (Figure 2c). Large plagioclase grains record evidence of plastic deformation, as shown by deformation twins, some of which are bent (Figure 2h). Garnet-clinopyroxene textures in SD2-LC71 appear to have formed by reaction (Farmer et al., 2005), as evidenced by intricate garnet-clinopyroxene coronas forming near and around orthopyroxene, plagioclase, and occasionally ilmenite. Note that garnet and clinopyroxene, together, constitute over 60% of the mineral mode (Table 1). Fine-grained corona clinopyroxene grains share similar crystallographic preferred orientations (based on IPF in the sample reference frame; Figure 2h) compared to

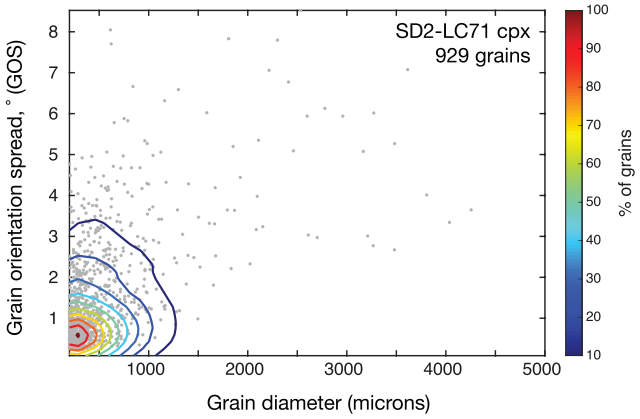

Figure 4. Grain orientation spread (GOS) versus grain size for 929 clinopyroxene grains in SD2-LC71. The GOS is similar to mis2mean but reports one value for each grain denoting the degree of internal misorientation (higher numbers represent more intragranular misorientation). Each gray point represents one grain. The data have been contoured using a 2-D histogram method to show that there are a large number of small grains with low GOS (these correspond to clinopyroxene inside garnet coronas) and a small number of large grains with high GOS (these correspond to clinopyroxene porphyroclasts).

coarser-grained clinopyroxene outside coronas. Interestingly, large clinopyroxene porphyroclasts appear to have higher degrees of lattice distortion compared to fine-grained clinopyroxene in garnet coronas. This is shown in the mis2mean (misorientation to the mean) map in Figure 2g and quantitatively in Figure 4. The mis2mean measures the extent of intragranular misorientation by plotting the difference of orientation (misorientation) between the crystal's average orientation and the measured orientation at a given point in the grain. Since crystal misorientations generally arise from dislocations, mis2mean maps provide a graphical representation of the extent of ductile deformation in a grain population.

4.3. Mineral Compositions: Major Elements and Water Content

Clinopyroxene major element compositions from Bradley and McCallum (1984) and Farmer et al. (2005) along with new data from four xenoliths (SD2-L110, SHE-1, SD2-LC71, and SD2-LC75) are plotted against MgO in Figure 5; all data are reported in SI Table S1. Clinopyroxenes are diopsidic with significant jadeitic components (Bradley & McCallum, 1984; Farmer et al., 2005) and generally unzoned with respect to major elements. The average H_2O content of clinopyroxene varies from 75 to 760 ppm and is inversely correlated with clinopyroxene Mg# (Figure 6 and Table 2). H_2O contents are relatively homogeneous within individual grains within a given xenolith (Figure S8); however,

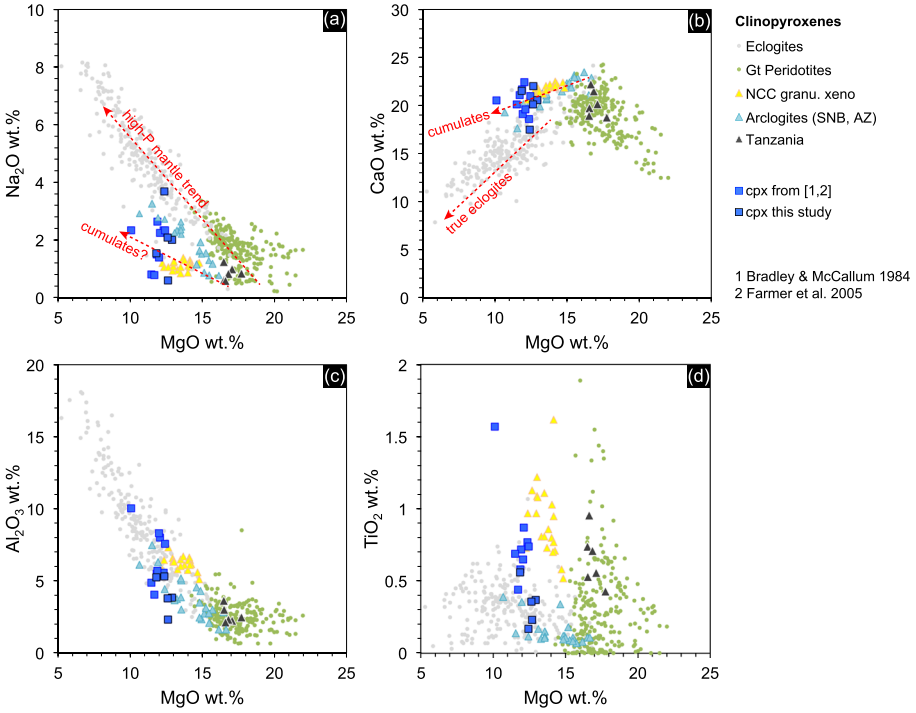

Figure 5. Clinopyroxene compositions. Clinopyroxene major element oxides plotted against MgO (wt.%). Dashed red lines highlight general trends followed by mantle rocks (high-P mantle trend, exemplified by mantle eclogites) and distinct trend followed by cumulates. Compositions of clinopyroxenes in eclogite xenoliths are from Hills and Haggerty (1989), Fung and Haggerty (1995), Beard et al. (1996). Compositions of clinopyroxenes in garnet peridotites are from Boyd and Mertzman (1987), Ehrenberg (1982), Hervig et al. (1986), Franz et al. (1996), Reid et al. (1975). (a) Na_2O versus MgO, (b) CaO versus MgO, (c) Al_2O_3 versus MgO, and (d) TiO_2 versus MgO.

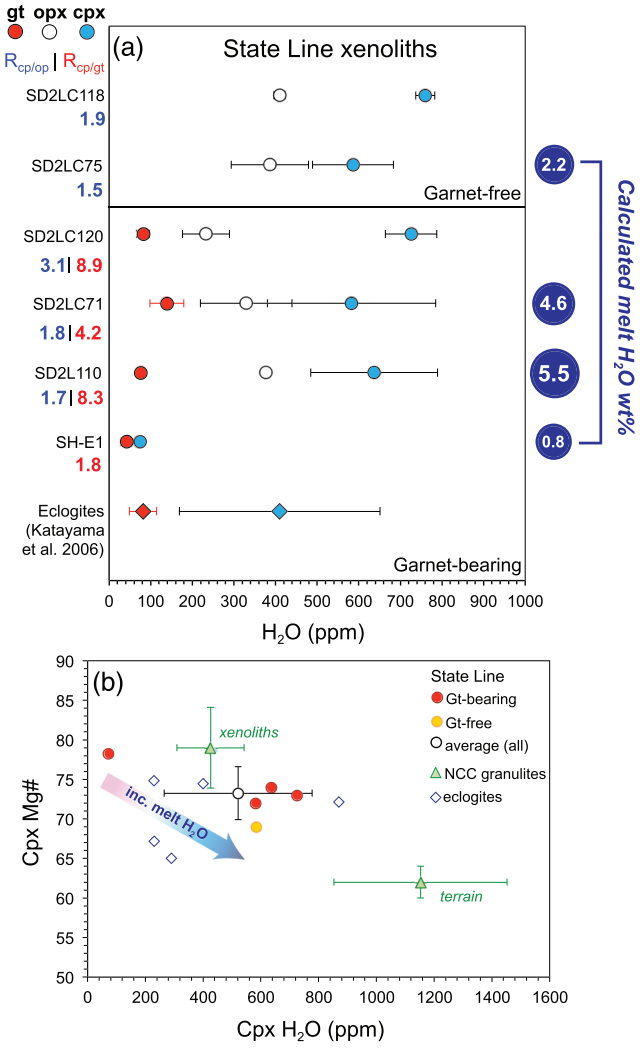

Figure 6. Water content in major silicate nominally anhydrous minerals. (a) H_2O (ppm) in garnet, orthopyroxene, and clinopyroxene in State Line lower crustal xenoliths. Intermineral ratios shown for cpx/opx and cpx/garnet on left side; calculated melt H_2O content shown on right side. See text for details. (b) Clinopyroxene Mg# versus clinopyroxene H_2O (ppm). NCC granulite data from Yang et al. (2008); eclogite data from Katayama et al. (2006). Shaded arrow shows calculated trend of increasing melt H_2O with decreasing Cpx Mg#.

some xenoliths show a range of H_2O concentrations across individual grains. Generally, grains are unzoned with respect to H_2O, but a few xenoliths show grains with slightly higher H_2O in cores versus rims.

We report new orthopyroxene major element compositions for SD2-LC75, SD2-LC71, and SD2-L110; these data as well as selected mineral data published in Bradley and McCallum (1984) and Farmer et al. (2005) are included in SI Table S1. Orthopyroxene is generally enstatitic (~70%) and unzoned with respect to major elements. Average H_2O content of orthopyroxene ranges from 233 to 410 ppm (Table 2).

Major elements were analyzed in garnet from SD2-LC71, SH-E1, and SD2-L110 and reported in SI Table S2. Garnets are pyrope-almandine. The average H_2O content of garnet varies from 42 to 139 ppm and is also inversely correlated with bulk rock Mg# and clinopyroxene Mg#. Garnets are unzoned with respect to H_2O and also quite homogeneous in major element composition within individual grain populations in a given xenolith (SI Tables S2 and S4).

In addition to the modally abundant minerals clinopyroxene, orthopyroxene, and garnet, we also analyzed H_2O contents in accessory minerals apatite, phlogopite, and amphibole. These are reported in SI Table 3.

4.4. Whole-Rock Major Element Systematics

Whole-rock major element oxides of 15 xenoliths previously reported in Bradley and McCallum (1984) and Farmer et al. (2005) are plotted against Mg# (atomic Mg/(Mg + FeT) * 100) in Figures 7a–7d. FeO_T and MgO are plotted against SiO_2 in Figures 7e and 7f, respectively. Broadly, the State Line lower crustal xenoliths are mafic, with Mg#s ranging from 51 to 69. Average SiO_2 contents are slightly lower (48.7 wt.%) than average MORB (50 wt.%). Notably, some xenoliths extend to low SiO_2 values <47 wt.% (Figure 7c). The State Line xenoliths also trend toward lower CaO with decreasing Mg# compared to average MORB (Figure 7e) and toward higher FeO with decreasing Mg#. We point out xenolith SH-E1, which was previously classified as MORB-type eclogite (Farmer et al., 2005) plots away from average MORB in terms of Al_2O_3 (10 wt.% compared to 15 wt.% for average MORB), MgO (13 wt.% vs. 7.5 wt.%), and Na_2O (2.2 wt.% vs. 2.6 wt.%) (Figure 7).

5. Discussion

5.1. Intermineral Partitioning of H_2O

To assess equilibrium with respect to H_2O contents between minerals, we compare intermineral ratios of measured H_2O concentrations ("*R*," Table 2) to experimental mineral/melt partition coefficients ("*D*"). Due to lack of published experimental H_2O partition coefficients for lower crustal rocks, we used experimental *D* values from Aubaud et al. (2004) and Tenner et al. (2009). Although these experiments pertain to mantle assemblages, our xenoliths have a broadly similar basaltic mineralogy, with the exception of olivine. We note, however, that published ranges of experimental H_2O mineral/melt partition coefficients are similar between plagioclase (0.001–0.006; Lin et al., 2019) and olivine (0.0013–0.0021; Hauri et al., 2006). Similar to mantle rocks, lower crustal rocks of broadly basaltic compositions contain abundant pyroxene, which has the highest DH_2O mineral/melt compared to olivine, plagioclase, and garnet. Thus, we can expect that H_2O partitioning between nominally anhydrous minerals in basaltic granulites to share some similarities with mafic and ultramafic upper mantle rocks.

Using average mineral water contents, *R*cpx/opx for garnet-free xenoliths SD2-LC118 and SD2-LC75 are 1.9 and 1.5, respectively (Figure 6 and Table 2). These values agree well with *D* values of 1.4 ± 0.3 for a

Table 2
H_2O Content (ppm) in NAMs, Intermineral Partitioning, and Reconstructed Bulk H_2O and Calculated Melt H_2O Contents

		SHE1	SD2L110	SD2LC71	SD2LC120	SD2LC75	SD2LC118
Garnet	Min	19	69	99	70		
	Max	67	102	230	104		
	Average	42	77	139	83		
	1σ	13	9.9	41	15		
	n	6	2	9	7		
Cpx	Min	62	476	345	634	486	733
	Max	96	1,225	1,178	835	766	775
	Average	75	637	583	726	586	760
	1σ	9.8	152	202	62	97	23
	n	11	9	11	3	5	2
Opx	Min		372	249	132	307	399
	Max		380	647	322	547	425
	Average		377	330	233	387	410
	1σ		4.4	110	56	93	14
	n		2	6	3	4	3
	R cpx/opx (avg)		1.7	1.8	3.1	1.5	1.9
	R cpx/gt (avg)	1.8	8.3	4.2	8.7		
	Bulk H_2O^a	58	406	291		242	
	Bulk H_2O^b (ppm)	82	651	564			
	Calc melt H_2O^a (wt.%)	0.8	5.5	4.6		2.2	

Note. n = number of individual grains analyzed; 1σ = 1 standard deviation calculated from total number of individual spots per mineral (at least three spots per grain).
[a]Reconstructed using average mineral H_2O contents. [b]Reconstructed using maximum mineral H_2O contents.

garnet-free basaltic assemblage at 1–2 GPa from Aubaud et al. (2004). *R*cpx/opx (using average values) for garnet-bearing xenoliths SD2-LC120, SD2-LC71, and SD2-L110 *R*cpx/opx are 3.1, 1.8, and 1.7 (Table 2), which also overlap with the range of *D*cpx/opx of 1.2 to 2 reported by Tenner et al. (2009) for garnet-bearing systems. Using average mineral water contents, *R*cpx/gt range from 1.8 to 8.3 (Table 2). If the maximum values for cpx and garnet water content is used, *R*cpx/gt range from 1.4 to 12. For comparison, experimental *D*cpx/gt range from 5.5 to 14 as reported in Tenner et al. (2009).

While the *R* values between minerals in our xenoliths show decent overlap with experimental *D*'s, the question arises as to whether the kimberlite eruption itself could have modified mineral H_2O concentrations. Addition of H_2O from the kimberlite magma into minerals was likely negligible, given that most individual mineral grains are homogeneous and unzoned with respect to H_2O. Furthermore, no correlation exists between mineral H_2O and grain size—if the host magma modified mineral H_2O, one might expect some correlation given that large grains should retain more H_2O and smaller grains either less H_2O (degassing) or gained H_2O (ingassing). A few clinopyroxene grains do show slightly lower H_2O at rims compared to cores, which could indicate either a limited extent of H_2O loss during eruption, or H_2O decrease due to subsolidus cooling (Chin et al., 2016). In summary, there is no evidence that H_2O was added to mineral grains during kimberlite eruption. While H_2O could have been lost from mineral grains during eruption, the observation that intermineral H_2O contents largely reflect equilibrium *D* values suggests that eruption-induced loss was also probably minimal (since kimberlites erupt on extremely rapid timescales). However, H_2O "loss"—or, alternatively, as we discuss later—decreased H_2O solubility within an approximate equilibrium state of subsolidus cooling, indicates that our measured H_2O contents are minimum bounds.

5.2. Reconstructed Bulk Rock H_2O and Calculated Melt H_2O

In the previous section, we established that intermineral H_2O ratios in the State Line xenoliths fall within range of experimental mineral/melt *D* values. This observation justifies our approach, described below, of calculating equilibrium melt H_2O contents that could have last been in equilibrium with our xenoliths.

Before further discussing recalculated bulk rock H_2O and hypothetical melt compositions, it is important to revisit the cooling history of the State Line lower crustal xenoliths and the impact on measured H_2O contents. Petrographic and textural observations of the xenoliths point to subsolidus cooling, such as the

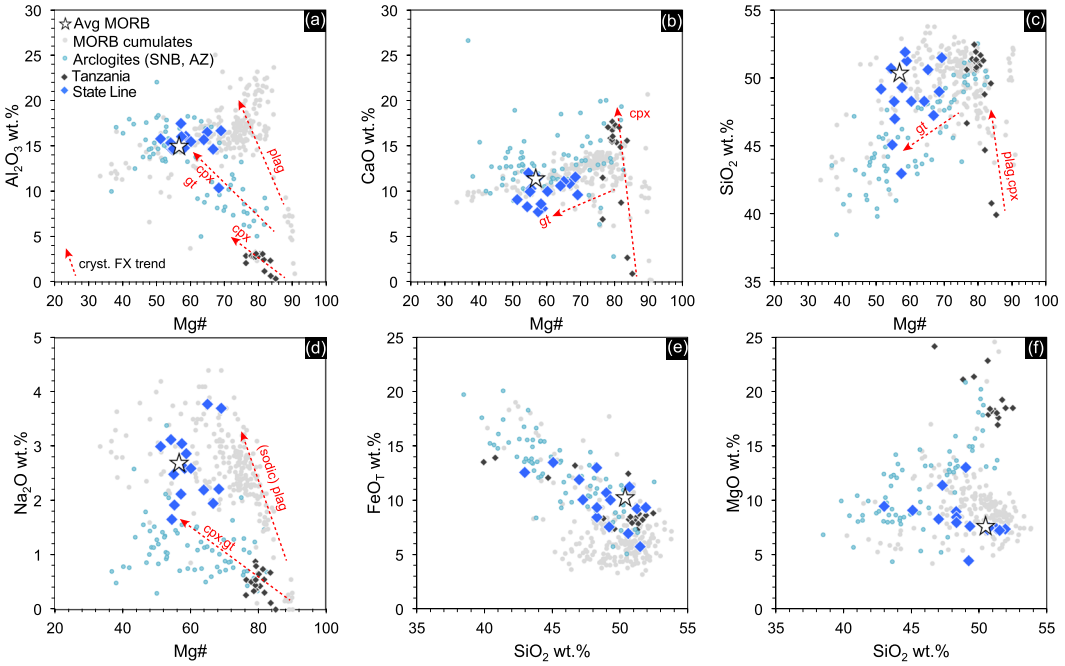

Figure 7. Whole-rock major element systematics. Whole-rock major element oxides of State Line lower crustal xenoliths. Also plotted for comparison are average MORB, MORB cumulates, arclogites, and intraplate rift cumulates (Tanzania). Dashed red lines are schematic trends corresponding to crystal fractionation of different minerals (plagioclase, clinopyroxene, etc.). (a) Al_2O_3 versus Mg#, (b) CaO versus Mg#, (c) SiO_2 versus Mg#, (d) Na_2O versus Mg#, (e) FeO_T versus SiO_2, and (f) MgO versus SiO_2.

abundance of garnet-clinopyroxene coronas interpreted to have formed at the expense of orthopyroxene and plagioclase (Farmer et al., 2005). Although coronas could result from increasing temperature and pressure (e.g., prograde metamorphism from medium to high-grade granulites), they have also been proposed to form via isobaric cooling (due to the slope of the spinel-garnet transition; Figure 8; Kushiro & Yoder, 1966) or cooling with increasing pressure (Chin et al., 2012; Saltzer et al., 2001). We consider that State Line xenoliths experienced subsolidus cooling following lower crustal stabilization sometime in the Proterozoic (as previously proposed by Farmer et al., 2005). If this is the case, H_2O contents measured in nominally anhydrous minerals likely represent minimum bounds, due to the lowering of H_2O solubility with decreasing temperature (cf. Zhao et al., 2004). Note that the effect of temperature on H_2O solubility is well constrained for olivine but not for pyroxenes. Unlike olivine, some mechanisms of water incorporation in pyroxene are thought to be coupled to slow-diffusing cations, such as the exchange $Al^{3+} + H^+ = Si^{4+}$; Keppler and Bolfan-Casanova (2006). Thus, it might be expected that the cooling effect on H_2O solubility may not be as extreme as that in olivine. Future experimental work may shed new insights into H_2O solubility in minerals other than olivine. What matters for the present study is that calculated melt H_2O contents using our measured H_2O contents and D values are likely to be minimum bounds due to cooling.

If we consider that subsolidus cooling could have decreased the absolute concentrations of H_2O in NAMs, but that cooling occurred such that intermineral H_2O ratios continued to reflect ambient equilibrium conditions (as observed in intermineral H_2O ratios), we can reconstruct bulk rock H_2O using maximum observed mineral H_2O contents as a way to "see past" the effect of cooling (cf. Chin et al., 2016). Although the spread of H_2O contents within individual mineral grains is low (i.e., negligible core-rim zoning), within individual xenoliths the H_2O contents of the grain population can be variable (Table 2, SI Figure S8, and SI Table S4) but does not vary more than ~30% (relative standard deviation [RSD]) within a given xenolith. For instance, clinopyroxene H_2O varies from a minimum of 476 ppm to a maximum of 1,225 ppm in SD2-L110; out of a population of nine clinopyroxene grains, only two grains had H_2O above the average value of 637 ppm for the whole population. Within those two grains with high H_2O, multiple

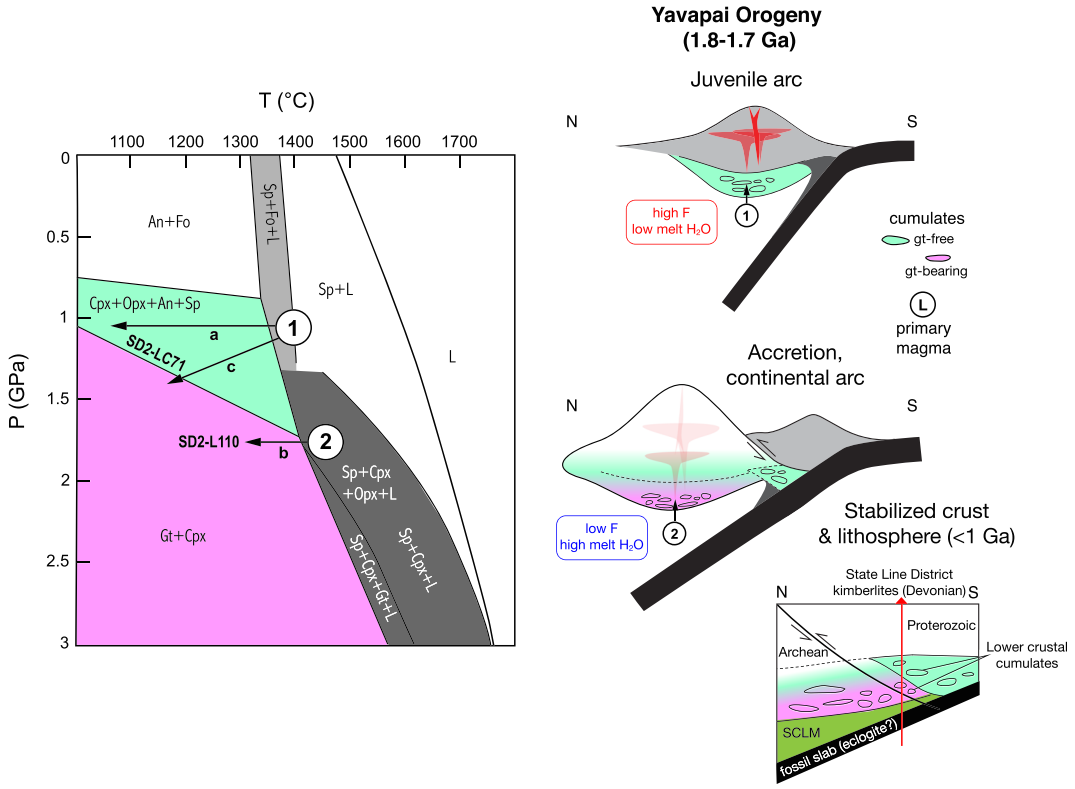

Figure 8. Petrologic and geologic interpretation. Phase diagram for a bulk composition of 1:1 molecular anorthite and forsterite, from Kushiro and Yoder (1966). Numbers 1 and 2 represent hypothetical protoliths of SD2-LC71 and SD2-L110, respectively. Number 1 is a magma with cpx, opx, spinel, and ±olivine on its liquidus; upon cooling it would crystallize cumulates with the mineralogy cpx + opx + plagioclase + spinel (green field − gabbros). Number 2 is a slightly higher pressure magma without olivine on the liquidus; upon cooling it would crystallize garnet + cpx cumulates. Paths a, b, and c represent possible subsolidus *P-T* paths. See text for details. (right) Proposed tectonic model associated with the Proterozoic Yavapai orogeny. Block diagram after Eggler et al. (1988) showing architecture of the crust and lithosphere following accretion and stabilization.

spots yielded reproducible results (within 15%). We also note that because of the time-resolved and in situ context of the SIMS measurements, any measurements that could have been contaminated by fluid inclusions or other impurities are easily resolved and can be removed during data reduction. Thus, we are confident that any grains with H_2O above the average value for a given xenolith are likely to be real and still reflect minimum bounds on the naturally preserved H_2O contents. Using maximum observed H_2O contents and mineral modes, reconstructed bulk rock H_2O range from 82 ppm (SH-E1) to 651 ppm (SD2-L110). In comparison, reconstructed bulk rock H_2O using average mineral H_2O values give a range from 58 to 406 ppm.

Next, we calculate H_2O contents of melts last in equilibrium with the bulk reconstructed xenolith H_2O contents (Table 2). To do so, we first determine a bulk DH_2O value for each xenolith using experimental D values and mineral modes, which is then used to calculate $C_{H2O\ melt}$. For garnet-bearing xenoliths, we determined melt water contents ranging from 0.8 wt.% (SH-E1) to 5.5 wt.% (SD2-L110) (using average mineral H_2O; if maximum mineral H_2O are used, calculated melt H_2O will be higher). We calculated melt water content of 2.2 wt.% for one garnet-free xenolith (SD2-LC75). Calculated melt H_2O contents increase with decreasing clinopyroxene Mg# and decreasing modal garnet and clinopyroxene. The calculated melt H_2O is noted next to each xenolith in Figure 6a.

5.3. A Cumulate, Arclogite Origin for the State Line Lower Crustal Suite

Previous studies on the State Line lower crustal granulite xenoliths lack clarity on the origin and tectonic setting of the protoliths. While all agreed the protolith had to be related to some form of basaltic

magmatism, three competing hypotheses as to the magmatic process responsible were proposed by Lester and Farmer (1998) and Farmer et al. (2005): cumulates, restites, or in situ crystallized basaltic melt. Eggler et al. (1988) interpreted the diverse xenolith systematics of the Colorado-Wyoming kimberlites as evidence of tectonically juxtaposed lithospheric domains: an Archean terrane containing abundant eclogite and a Proterozoic terrane dominated by peridotite and lower crustal rocks. However, this lithospheric structure was most likely further complicated by the various subduction and accretion events that took place along the southern border of the Wyoming Craton throughout the Proterozoic.

Using our new data on H_2O concentrations in NAMs in the State Line xenoliths, we provide new insights into the nature of the protoliths and their tectonic setting. A key finding from our analysis of the H_2O data is that the *minimum* water content of the melt last in equilibrium with the most primitive xenolith is already quite hydrous (~1 wt.% H_2O) compared to typical primitive MORB (~0.1 wt.%; Sobolev & Chaussidon, 1996). Calculated melt water contents increase with decreasing Mg# (Figure 6b), consistent with a fractional crystallization trend wherein the xenoliths could represent (now metamorphosed) crystal cumulates. While a similar trend might also be predicted for a restite (partial melting) trend, we might expect mineral and bulk rock H_2O contents to be even lower than observed if significant partial melting occurred, which should effectively remove all or most of the water. It is also unlikely that the State Line xenoliths represent "frozen in" basaltic melts trapped at depth, if we assume that their protoliths were MORB-like in terms of H_2O content, as has been proposed for some arc basement in the Colorado Province (Cavosie & Selverstone, 2003). Moreover, if MORB-like melts crystallized at initially shallow pressures and then cooled during accretion and thickening, as proposed by Cavosie and Selverstone (2003), we should expect bulk rock H_2O contents less than or equal to typical water contents of primitive MORBs, which are at least 10 times lower than our reconstructed bulk rock H_2O contents. Thus, we propose that the State Line lower crustal xenoliths represent cumulates from a hydrous melt.

Comparison of the State Line lower crustal xenoliths with other deep crustal cumulates also supports an origin by crystal fractionation from hydrous magmas. Although the overall major element composition of most of the xenoliths would place them within the field of typical MORB olivine tholeiite (Bradley & McCallum, 1984; Lester & Farmer, 1998), from Figure 7 it is apparent that over 50% of the xenoliths have whole-rock Mg#'s greater than average MORB. In addition, the CaO and SiO_2 content of most State Line lower crustal xenoliths are lower than average MORB (Figures 7b and 7c). FeO_T contents of the xenoliths also extend to higher values than average MORB (Figure 7e). The State Line lower crustal xenoliths also generally do not fall within the field of global MORB cumulates. Although the mean Mg# of MORB cumulates (71; Chin et al., 2018) is higher than the mean Mg# of the State Line xenoliths (60), the major element trends of the State Line xenoliths differ from MORB cumulates. For instance, the State Line xenoliths do not show Al_2O_3 enrichment at high Mg# signifying cotectic olivine + plagioclase crystallization characteristic of MORB cumulates. This is manifested modally by the absence of olivine in the State Line xenoliths. The State Line xenoliths also plot in regions distinct from MORB cumulates in SiO_2 versus Mg# and Na_2O versus Mg# plots (Figures 7c and 7d).

The State Line xenoliths do overlap compositionally with the Sierran and Arizona arclogite xenolith field. Arclogites are distinct from eclogites, the former representing garnet and pyroxene-rich cumulates from primitive, hydrous arc magmas (Lee & Anderson, 2015), whereas the latter are metamorphosed equivalents of basalt. The mean Mg# of 60 for State Line xenoliths is similar to the range reported for low-MgO garnet pyroxenites from the Sierra Nevada (Lee et al., 2006) and also the mean of ~62 for island and continental arcs (Chin et al., 2018). Furthermore, the State Line xenoliths have similar Al_2O_3 at a given Mg# range as low-MgO arclogites (Figure 7a); their FeOT contents also extend to elevated values similar to arclogites (Figure 7e) and in contrast to Fe-poor MORB cumulates. CaO contents are overall similar, but slightly lower, than arclogite xenoliths (Figure 7b). Although the SiO_2 content shows a wide range from 43 to 52 wt.%, approximately half of the State Line xenoliths have SiO_2 overlapping with Sierran and Arizona arclogites.

We compare clinopyroxene compositions from the State Line xenoliths to other published data on deep lithospheric clinopyroxenes. These include clinopyroxenes from global peridotite and eclogite xenoliths (see Figure 5 caption for references), arclogites from Mesozoic arcs in western North America (Erdman et al., 2016; Lee et al., 2006), intraplate clinopyroxenite cumulates from Tanzania (Chin, 2018), and granulite xenoliths from the lower crust of the North China Craton (Yang et al., 2008). The State Line clinopyroxenes

clearly fall off the high-pressure mantle array represented by garnet peridotite and eclogite xenoliths; the former are confined to a narrow range of Na_2O and CaO contents, while the latter trend toward high Na_2O and low CaO (Figures 5a and 5b). Clinopyroxene from granulite xenoliths from North China are also distinct from the State Line clinopyroxenes. This could be attributed to the lower modal abundance of garnet in the North China granulites—most of these granulites are garnet-free, and those that contain garnet have it in abundances of 25% or less (Yang et al., 2008), in contrast to garnet-bearing State Line xenoliths, which have >25% garnet. Again, similar to bulk rock trends, State Line clinopyroxenes overlap most with clinopyroxenes from low-MgO garnet pyroxenites from arclogite xenoliths. Similarities between State Line and low-MgO arclogite clinopyroxenes are most clear in Na_2O versus MgO, CaO versus MgO, and Al_2O_3 versus MgO (Figures 5a–5c). TiO_2 contents are overall higher than arclogite clinopyroxene, but the steep vertical trend in the TiO_2 versus MgO plot is similar to steep trends observed in other cumulate-type rocks (e.g., North China and Tanzania). One possibility for the discrepancy in TiO_2 between State Line and arclogite clinopyroxene is that in many arclogites, rutile was reported as an exsolution product from garnet and clinopyroxene (Erdman et al., 2016; Lee et al., 2006).

5.4. Deep, Hydrous Fractional Crystallization

Based on the discussion above, H_2O systematics, whole-rock, and clinopyroxene compositional data all suggest that the State Line lower crustal xenoliths could represent crystal cumulates from primitive, hydrous magmas. Crystallization experiments of hydrous basaltic andesites at deep crustal conditions (~1 GPa) produced cumulates with variable amounts of garnet, plagioclase, hornblende, clinopyroxene, and orthopyroxene (Muntener & Ulmer, 2006), broadly similar (with the exception of hornblende) to our xenoliths. The prevalence of hornblende in the experiments is probably due to the relatively high melt H_2O contents in the starting material (4–8 wt.%). Hornblende may have once been present in our xenoliths prior to final equilibration in the granulite facies, and hornblende is present in small amounts in some xenoliths (Farmer et al., 2005).

Olivine-hosted melt inclusions from subduction zones worldwide show a well-defined average H_2O content of 3.9 wt.% ± 0.4 (Plank et al., 2013). We calculated 5.5 and 4.6 wt.% H_2O in melts equilibrated with garnet-bearing xenoliths SD2-L110 and SD2-LC71 (Table 2 and Figure 6). However, melt inclusions have likely undergone diffusive H_2O loss during ascent (Bucholz et al., 2013), and most melt inclusions appear to have last equilibrated within the midcrust (~6 km; Plank et al., 2013), shallower than lower crustal cumulate xenoliths. Thus, it may not be straightforward to compare H_2O contents measured in melt inclusions and H_2O estimated from cumulates. The former may simply reflect vapor saturation at their last depth of equilibration prior to eruption (Plank et al., 2013), whereas the latter reflect a minimum bound on magmatic H_2O because of the effects of subsolidus cooling. Melt inclusions hosted in the most primitive olivines ($>Fo_{86}$) have higher H_2O than those in $<Fo_{85}$ olivine (Plank et al., 2013), with some values as high as ~6 wt.% H_2O (Figure 1 in Plank et al., 2013). Although the State Line xenoliths do not contain olivine, they have clinopyroxene with Mg#'s ranging from 64 to 84 (Figure 6 and SI Table S1), similar to clinopyroxene from experimental mafic arc cumulates (Alonso-Perez et al., 2009) and overlapping some low-MgO garnet pyroxenites from the Sierra Nevada (Lee et al., 2006). The Sierran low-MgO garnet pyroxenites most likely equilibrated at depths <1 GPa and reflect a second, shallower stage of hydrous cumulate fractionation (Lee et al., 2006). Although our comparisons have large uncertainties, our xenolith-constrained estimates of ~1 to 5.5 wt.% H_2O in the melt show agreements with global melt inclusions systematics.

While in a broad sense, we interpret the State Line lower crustal xenoliths to represent cumulates from primitive, hydrous melts, it is unclear whether all the xenoliths in the suite represent one crystal line of descent from a single parent magma, or "instantaneous" cumulates from various (but petrologically similar) magmas. Due to the nature of xenolith sampling, it is probably impossible to answer this question. Thus, it is possible that the ~5 wt.% melt H_2O we calculated for garnet-bearing xenoliths SD2L-110 and SD2LC-71 (Table 2) could reflect a "snapshot" of part of the crystal line of descent, and so melt H_2O would be expected to vary where a given cumulate is along that line of descent. One way to "see through" to the H_2O content of the parental magma is to consider the most primitive (highest Mg#) cumulates, as these cumulates would have fractionated out early along the magmatic differentiation path. If we consider the most primitive xenolith in our suite, SH-E1 (highest clinopyroxene Mg#) as one of the earliest crystal cumulates to fractionate

from a hydrous basaltic melt, the observed mineral modes match the near bimineralic assemblages of early experimental cumulates (Alonso-Perez et al., 2009) as well as natural cumulate arclogites (Lee et al., 2006). Using a simple Rayleigh fractional crystallization model, assuming we start with 1 wt.% H_2O in the melt (although we calculated 0.8 wt.% H_2O in equilibrium SH-E1, we use 1 wt.% for simplicity; using 0.8 wt.% does not change the final result significantly), a fractionating assemblage of clinopyroxene and garnet in ratios ranging from 50:50 to 25:75, and a $D_{bulk} = 0.004$, and allowing this melt to crystallize to $F = 0.4$ results in melt H_2O of ~4 wt.%. Thus, even "low" initial melt H_2O contents can still evolve relatively hydrous magmas. We emphasize that this process is possible in the deep crust. Mafic melts have low critical melt fractions, <20% (Paterson et al., 1998)—and so melt extraction could occur at lower crystallinities and generally be more efficient compared to more silicic melts. This would be facilitated even more with hydrous melts, owing to the high incompatibility of water; if early melts have high initial H_2O, with increasing crystal fractionation, they will become even more enriched in H_2O. This could be one way that deep crustal fractional crystallization sets the stage for further magmatic evolution in the middle crust, where amphibole can become stable at high melt H_2O contents (Davidson et al., 2007).

5.5. Geologic and Tectonic Implications

Though now metamorphosed into the granulite facies, we propose that the State Line lower crustal xenoliths were originally crystal cumulates from hydrous melts. The presence of both garnet-free, plagioclase-bearing xenoliths and garnet and clinopyroxene-rich xenoliths could represent two magmatic lineages with lower and higher melt H_2O contents, respectively. One geologic scenario that could explain this dichotomy is the following. The Yavapai arc terrane is thought to represent products of oceanic island arc magmatism that accreted onto the North American continent during the Yavapai Orogeny (1.8–1.7 Ga). During oceanic island arc magmatism, the lithosphere (as a whole) is generally under extension, and crustal thickness tends to be lower than that in continental arcs (Chin et al., 2018). Thus, average degree of melting at thin crust arcs can be moderate to high, producing primary melts at shallower pressures and with lower melt H_2O (1 in Figure 8). Such melts might fall more along a tholeiitic trend and would produce cumulates composed mostly of pyroxene and plagioclase (gabbros).

The Yavapai arc system may have evolved to a continental arc as the terrane sutured onto North America; Proterozoic calc-alkaline plutons in the vicinity of the State Line District may be evidence of this (Karlstrom & Houston, 1984). Cavosie and Selverstone (2003) proposed that the ~1.7 Ga arc magmatism of the Colorado province may have been built initially on oceanic crust, which originated either as a ridge-transform intersection or a backarc spreading center, and then was subsequently entrapped during accretion of the Yavapai terrane onto the Wyoming Craton. During this transition, the crust presumably thickened, resulting in progressively deeper melt generation depths, thus lower degrees of melting (Plank & Langmuir, 1988), and hence higher initial melt H_2O (Chin et al., 2018). Such higher-H_2O and higher pressure melts would crystallize liquidus garnet and clinopyroxene as early cumulates (2 in Figure 8), represented now in the State Line xenoliths as the garnet-rich granulites. The scenario proposed above could also explain the transitional nature of the State Line lower crustal xenolith suite, which shows gradation from gabbros (tholeiitic trend) to more garnet and clinopyroxene-rich assemblages (calc-alkaline trend). Following cooling into the granulite facies, the Proterozoic State Line lower crust stabilized and was subsequently tectonically juxtaposed over Archean lithosphere (Eggler et al., 1988) and then sampled by kimberlites in the Devonian (Figure 8).

The occurrence of abundant garnet-pyroxene coronas is also consistent with two, or possibly more, distinct arc magma lineages that subsequently experienced *P-T* paths governed by where they started along the solidus in Figure 8. Analysis of the phase boundaries in Figure 8 shows that near-solidus cumulates of a low pressure, tholeiitic Melt 1 in Figure 8 would have to cool to a large extent to enter the garnet stability field due to the slope of the spinel-garnet transition (Path a). Note that garnet formation solely due to isobaric cooling of plagioclase-rich protoliths, such as Composition 1 in Figure 8, is kinetically inefficient (Chapman et al., 2017). This could explain the substantial population of plagioclase-bearing granulites in the State Line suite. By contrast, near-solidus cumulates of a deeper, presumably more calc-alkaline and hydrous, Melt 2 in Figure 8 would already have spinel, clinopyroxene ± orthopyroxene, and garnet as liquidus phases, and a smaller extent of cooling would immediately precipitate garnet and clinopyroxene as early cumulate minerals, like xenolith SD2-L110 (Path b). Alternatively, a protolith starting at 1 in Figure 8 could

undergo an increase in pressure while cooling (Path c) (Chin et al., 2016), which would pivot more quickly to the garnet stability field due to the slope of the garnet-in boundary, allowing coronas to form without a large amount of cooling. This could be the case for SD2-LC71 and the "mixed" granulites that contain various proportions of plagioclase but abundant garnet + cpx coronas.

Our EBSD data also suggest a history more complex than simple isobaric cooling for the corona-bearing xenoliths. Microstructural observations in SD2-LC71 show abundant deformation twins in plagioclase porphyroclasts, and large clinopyroxene grains more deformed than fine-grained clinopyroxene inside garnet coronas (Figures 2g and 4), suggesting that delicate corona structures formed after an earlier ductile deformation. Such a two-stage deformation history could be explained by a thickening + cooling path. We conclude that isobaric cooling alone—a *P-T* path typically associated with mafic underplating—is likely not sufficient to account for the high modal garnet (>25%) and clinopyroxene (>30%) in many of the State Line xenoliths. Together with H_2O contents in NAMs consistent with an igneous cumulate heritage and microstructural evidence of a complex deformation history encapsulated between ~1.8 and ~400 Ma, we therefore propose that the State Line granulites represent deep remnants of continental crust formed in an evolving arc setting in the Proterozoic.

Finally, while garnet-rich arc cumulates are critical for facilitating delamination or convective removal of thickened arc roots (Lee & Anderson, 2015), it should not go unnoticed that plagioclase-bearing cumulates are also an important constituent of igneous arc lithosphere. The origin of these gabbroic cumulates is less clear, since they could have formed either in juvenile arcs that were subsequently accreted or perhaps at oceanic ridges. The buoyancy of gabbroic cumulates relative to garnet-bearing cumulates may allow them to survive capture and suturing, thereby providing a buoyant "life raft" onto which subsequent calc-alkaline continental arc magmatism may grow upon. In the Sierra Nevada Batholith, archetype of a continental arc, Ducea and Saleeby (1996) showed that gabbros, cumulate gabbros, and plagioclase granulites are nearly as abundant as garnet clinopyroxenites within the well-studied Sierra Nevada deep lithospheric xenolith suite. They further note that compositionally, the gabbroic cumulates and granulites overlap in terms of major element bulk composition with garnet clinopyroxenites, indicating a similar gradational spectrum observed in the State Line lower crust.

Parallels between the State Line xenoliths with Phanerozoic arclogites suggests that arcs could have operated in a similar manner in the Proterozoic. Our data on the H_2O content of granulite-facies rocks—typically thought to be "bone dry"—indicates that such rocks can contain significant H_2O: up to ~1,000 ppm in clinopyroxene and bulk H_2O up to ~650 ppm. Such values are at least a factor of 2 higher than maximum estimates for the upper mantle, the layer directly beneath the lower crust. Moreover, our measured H_2O contents are likely to be minimum bounds due to decreased solubility during cooling. This implies that lower crust formed in Proterozoic arcs could have been just as hydrous or even more hydrous than what is observed today.

6. Conclusions

We investigated the water contents of nominally anhydrous minerals, as well as modal mineralogy and rock microstructure, in lower crustal xenoliths from the State Line kimberlite district in northern Colorado, USA. Average water contents for minerals range from 75 to 760, 233 to 410, and 42 to 139 ppm for clinopyroxene, orthopyroxene, and garnet, respectively. Despite subsolidus cooling, intermineral water partitioning largely reflects equilibrium *D* values, indicating closed system conditions. Importantly, the coherence between measured intermineral partitioning and *D* values allows us to constrain minimum bounds on water contents of melts last in equilibrium with the xenoliths. Calculated melt water contents range from ~1 to ~6 wt.%. Together with the high garnet and clinopyroxene mode in many of the xenoliths and their overall resemblance to arclogite xenoliths from well-known arcs, we interpret the State Line xenoliths to have originally been igneous cumulates from moderate to high-pressure, hydrous magmas associated with arc magmatism during Proterozoic accretion of North America.

Conflict of Interest

The authors declare no financial interests that could be perceived as being a conflict of interest.

Data Availability Statement

All data in this publication are archived online (at https://doi.org/10.26022/IEDA/111662).

Acknowledgments
The authors are grateful for constructive reviews from Richard Palin and Tomoaki Morishita and to Editor Stephen Parman for handling the manuscript. E. J. C. thanks Joe Boesenberg for assistance on the Brown University EPMA and Lonnie Hufford for EBSD assistance. E. J. C. and S. T. C. thank Yunbin Guan for help on SIMS. This work was supported by grants from the National Science Foundation to E. J. C. (NSF EAR 1719208 and NSF EAR 1855407).

References

Alonso-Perez, R., Muntener, O., & Ulmer, P. (2009). Igneous garnet and amphibole fractionation in the roots of island arcs: Experimental constraints on andesitic liquids. *Contributions to Mineralogy and Petrology*, *157*(4), 541–558. https://doi.org/10.1007/s00410-008-0351-8

Arndt, N. T. (2013). The formation and evolution of the continental crust. *Geochemical Perspectives*, *2*(3), 405–533. https://doi.org/10.7185/geochempersp.2.3

Ater, P. C., Eggler, D. H., & McCallum, M. (1984). Petrology and geochemistry of mantle eclogite xenoliths from Colorado-Wyoming kimberlites: Recycled ocean crust? In J. Kornprobst (Ed.), *Developments in petrology* (Vol. 11, pp. 309–318). Elsevier. https://doi.org/10.1016/B978-0-444-42274-3.50032-9

Aubaud, C., Hauri, E. H., & Hirschmann, M. M. (2004). Hydrogen partition coefficients between nominally anhydrous minerals and basaltic melts. *Geophysical Research Letters*, *31*, L20611. https://doi.org/10.1029/2004GL021341

Aubaud, C., Withers, A. C., Hirschmann, M. M., Guan, Y., Leshin, L. A., Mackwell, S. J., & Bell, D. R. (2007). Intercalibration of FTIR and SIMS for hydrogen measurements in glasses and nominally anhydrous minerals. *American Mineralogist*, *92*(5–6), 811–828. https://doi.org/10.2138/am.2007.2248

Avé Lallemant, H. G. (1969). Structural and petrofabric analysis of an "alpine-type" peridotite: The lherzolite of the French Pyrenees. *Leidse Geologische Mededelingen*, *42*, 1–57.

Beard, B., Fraracci, K. N., Clayton, R. A., Mayeda, T. K., Snyder, G., Sobolev, N., & Taylor, L. (1996). Petrography and geochemistry of eclogites from the Mir kimberlite, Yakutia, Russia. *Contributions to Mineralogy and Petrology*, *125*(4), 293–310. https://doi.org/10.1007/s004100050223

Bickford, M., Van, W., & Zietz, I. (1986). Proterozoic history of the midcontinent region of North America. *Geology*, *14*(6), 492–496. https://doi.org/10.1130/0091-7613(1986)14<492:PHOTMR>2.0.CO;2

Boyd, F. R., & Mertzman, S. A. (1987). Composition and structure of the Kaapvaal lithosphere, southern Africa. In B. O. Mysen (Ed.), *Magmatic processes: Physicochemical principles* (pp. 13–25). University Park, PA: The Geochemical Society.

Bradley, S. D. (1985). *Granulite-facies and related xenoliths from Colorado-Wyoming kimberlite* (p. 148). Fort Collins, CO: Colorado State University.

Bradley, S. D., & McCallum, M. E. (1984). Granulite facies and related xenoliths from Colorado-Wyoming kimberlite. In J. Kornprobst (Ed.), *Developments in petrology* (pp. 205–217). Elsevier. https://doi.org/10.1016/B978-0-444-42274-3.50023-8

Bucholz, C. E., Gaetani, G. A., Behn, M. D., & Shimizu, N. (2013). Post-entrapment modification of volatiles and oxygen fugacity in olivine-hosted melt inclusions. *Earth and Planetary Science Letters*, *374*, 145–155. https://doi.org/10.1016/j.epsl.2013.05.033

Cavosie, A., & Selverstone, J. (2003). Early Proterozoic oceanic crust in the northern Colorado Front Range: Implications for crustal growth and initiation of basement faults. *Tectonics*, *22*(2), 1015. https://doi.org/10.1029/2001TC001325

Chapman, T., Clarke, G. L., Piazolo, S., & Daczko, N. R. (2017). Evaluating the importance of metamorphism in the foundering of continental crust. *Scientific Reports*, *7*, 1–12.

Chin, E. J. (2018). Deep crustal cumulates reflect patterns of continental rift volcanism beneath Tanzania. *Contributions to Mineralogy and Petrology*, *173*(10), 85. https://doi.org/10.1007/s00410-018-1512-z

Chin, E. J., Lee, C.-T. A., Luffi, P., & Tice, M. (2012). Deep lithospheric thickening and refertilization beneath continental arcs: Case study of the P, T and compositional evolution of peridotite xenoliths from the Sierra Nevada, California. *Journal of Petrology*, *53*(3), 477–511. https://doi.org/10.1093/petrology/egr069

Chin, E. J., Shimizu, K., Bybee, G. M., & Erdman, M. E. (2018). On the development of the calc-alkaline and tholeiitic magma series: A deep crustal cumulate perspective. *Earth and Planetary Science Letters*, *482*, 277–287. https://doi.org/10.1016/j.epsl.2017.11.016

Chin, E. J., Soustelle, V., Hirth, G., Saal, A., Kruckenberg, S. C., & Eiler, J. (2016). Microstructural and geochemical constraints on the evolution of deep arc lithosphere. *Geochemistry, Geophysics, Geosystems*, *17*, 2497–2521. https://doi.org/10.1002/2015GC006156

Collins, W. J., Murphy, J. B., Johnson, T. E., & Huang, H.-Q. (2020). Critical role of water in the formation of continental crust. *Nature Geoscience*, 1–8.

Condie, K. C. (1999). Mafic crustal xenoliths and the origin of the lower continental crust. *Lithos*, *46*(1), 95–101. https://doi.org/10.1016/S0024-4937(98)00056-5

Davidson, J., Turner, S., Handley, H., Macpherson, C., & Dosseto, A. (2007). Amphibole "sponge" in arc crust? *Geology*, *35*(9), 787–790. https://doi.org/10.1130/G23637A.1

Defant, M. J., & Drummond, M. S. (1990). Derivation of some modern arc magmas by melting of young subducted lithosphere. *Nature*, *347*(6294), 662–665. https://doi.org/10.1038/347662a0

Dickinson, W. R., & Snyder, W. S. (1978). Plate tectonics of the Laramide orogeny. In V. Matthews (Ed.), *Laramide folding associated with basement block faulting in the Western United States*, *Geological Society of America Memoir* (Vol. 151, pp. 355–366). https://doi.org/10.1130/MEM151-p355

Ducea, M. N. (2002). Constraints on the bulk composition and root foundering rates of continental arcs: A California arc perspective. *Journal of Geophysical Research*, *107*(B11), 2304. https://doi.org/10.1029/2001JB000643

Ducea, M. N., & Saleeby, J. B. (1996). Buoyancy sources for a large, unrooted mountain range, the Sierra Nevada, California: Evidence from xenolith thermobarometry. *Journal of Geophysical Research*, *101*(B4), 8229–8244. https://doi.org/10.1029/95JB03452

Eggler, D., Meen, J., Welt, F., Dudas, F. O., Furlong, K., McCallum, M., & Carlson, R. (1988). Tectonomagmatism of the Wyoming province. *Colorado School of Mines Quarterly*, *83*, 25–40.

Eggler, D. H., McCallum, M., & Kirkley, M. (1987). Kimberlite-transported nodules from Colorado-Wyoming. A record of enrichment of shallow portions of an infertile lithosphere. *Geological Society of America Special Paper*, *215*, 77–90.

Ehrenberg, S. N. (1982). Petrogenesis of garnet lherzolite and megacrystalline nodules from the Thumb, Navajo volcanic field. *Journal of Petrology*, *23*(4), 507–547. https://doi.org/10.1093/petrology/23.4.507

Erdman, M. E., Lee, C.-T. A., Levander, A., & Jiang, H. (2016). Role of arc magmatism and lower crustal foundering in controlling elevation history of the Nevadaplano and Colorado Plateau: A case study of pyroxenitic lower crust from central Arizona, USA. *Earth and Planetary Science Letters*, *439*, 48–57. https://doi.org/10.1016/j.epsl.2016.01.032

Farmer, G. L., Bowring, S. A., Williams, M. L., Christensen, N. I., Matzel, J. P., & Stevens, L. (2005). *Contrasting lower crustal evolution across an Archean-Proterozoic suture: Physical, chemical and geochronologic studies of lower crustal xenoliths in southern Wyoming and northern Colorado*, *Geophysical Monograph Series* (Vol. 154, pp. 139–162). Washington DC: American Geophysical Union.

Farmer, G. L., Fritz, D. E., & Glazner, A. F. (2020). Identifying metasomatized continental lithospheric mantle involvement in Cenozoic magmatism from Ta/Th values, southwestern North America. *Geochemistry, Geophysics, Geosystems*, *21*, e2019GC008499. https://doi.org/10.1029/2019GC008499

Franz, L., Brey, G. P., & Okrusch, M. (1996). Steady state geotherm, thermal disturbances, and tectonic development of the lower lithosphere underneath the Gibeon Kimberlite Province, Namibia. *Contributions to Mineralogy and Petrology*, *126*(1–2), 181–198. https://doi.org/10.1007/s004100050243

Fung, A. T., & Haggerty, S. E. (1995). Petrography and mineral compositions of eclogites from the Koidu Kimberlite Complex, Sierra Leone. *Journal of Geophysical Research*, *100*(B10), 20,451–20,473. https://doi.org/10.1029/95JB01573

Hauri, E. H., Gaetani, G. A., & Green, T. H. (2006). Partitioning of water during melting of the Earth's upper mantle at H_2O-undersaturated conditions. *Earth and Planetary Science Letters*, *248*(3–4), 715–734. https://doi.org/10.1016/j.epsl.2006.06.014

Hervig, R. L., Smith, J. V., & Dawson, J. B. (1986). Lherzolite xenoliths in kimberlites and basalts: Petrogenetic and crystallochemical significance of some minor and trace elements in olivine, pyroxenes, garnet and spinel. *Earth and Environmental Science Transactions of the Royal Society of Edinburgh*, *77*(3), 181–201. https://doi.org/10.1017/S026359330001083X

Hills, D. V., & Haggerty, S. E. (1989). Petrochemistry of eclogites from the Koidu kimberlite complex, Sierra Leone. *Contributions to Mineralogy and Petrology*, *103*(4), 397–422. https://doi.org/10.1007/BF01041749

Hirth, G., & Kohlstedt, D. L. (1995). Experimental constraints on the dynamics of the partially molten upper mantle: 2. Deformation in the dislocation creep regime. *Journal of Geophysical Research*, *100*, 15441–15449.

Humphreys, E., Hessler, E., Dueker, K., Farmer, G., Erslev, E., & Atwater, T. (2003). How Laramide-age hydration of North American lithosphere by the Farallon slab controlled subsequent activity in the western United States. *International Geology Review*, *45*(7), 575–595. https://doi.org/10.2747/0020-6814.45.7.575

Jagoutz, O. E. (2010). Construction of the granitoid crust of an island arc. Part II: A quantitative petrogenetic model. *Contributions to Mineralogy and Petrology*, *160*, 359–381.

Jones, C. H., Mahan, K. H., Butcher, L. A., Levandowski, W. B., & Farmer, G. L. (2015). Continental uplift through crustal hydration. *Geology*, *43*(4), 355–358. https://doi.org/10.1130/G36509.1

Karlstrom, K., & Houston, R. (1984). The Cheyenne belt: Analysis of a Proterozoic suture in southern Wyoming. *Precambrian Research*, *25*(4), 415–446. https://doi.org/10.1016/0301-9268(84)90012-3

Katayama, I., Nakashima, S., & Yurimoto, H. (2006). Water content in natural eclogite and implication for water transport into the deep upper mantle. *Lithos*, *86*(3–4), 245–259. https://doi.org/10.1016/j.lithos.2005.06.006

Keppler, H., & Bolfan-Casanova, N. (2006). Thermodynamics of water solubility and partitioning. *Reviews in Mineralogy and Geochemistry*, *62*(1), 193–230. https://doi.org/10.2138/rmg.2006.62.9

Kushiro, I., & Yoder, H. Jr. (1966). Anorthite–forsterite and anorthite–enstatite reactions and their bearing on the basalt–eclogite transformation. *Journal of Petrology*, *7*(3), 337–362. https://doi.org/10.1093/petrology/7.3.337

Kushiro, I., & Yoder, H. S. (1969). Melting of forsterite and enstatite at high pressures under hydrous conditions. *Carnegie Inst Washington Yearbook*, *67*, 153–161.

Lange, R. A., Carmichael, I. S., & Hall, C. M. (2000). $^{40}Ar/^{39}Ar$ chronology of the Leucite Hills, Wyoming: Eruption rates, erosion rates, and an evolving temperature structure of the underlying mantle. *Earth and Planetary Science Letters*, *174*(3–4), 329–340. https://doi.org/10.1016/S0012-821X(99)00267-8

Lee, C. T. A. (2014). 4.12—Physics and chemistry of deep continental crust recycling A2—Holland, Heinrich D. In K. K. Turekian (Ed.), *Treatise on geochemistry* (Second ed., pp. 423–456). Oxford: Elsevier. https://doi.org/10.1016/B978-0-08-095975-7.00314-4

Lee, C.-T. A., & Anderson, D. L. (2015). Continental crust formation at arcs, the arclogite "delamination" cycle, and one origin for fertile melting anomalies in the mantle. *Science Bulletin*, 1–16.

Lee, C.-T. A., Cheng, X., & Horodyskyj, U. (2006). The development and refinement of continental arcs by primary basaltic magmatism, garnet pyroxenite accumulation, basaltic recharge and delamination: Insights from the Sierra Nevada. *Contributions to Mineralogy and Petrology*, *151*(2), 222–242. https://doi.org/10.1007/s00410-005-0056-1

Lester, A., & Farmer, G. L. (1998). Lower crustal and upper mantle xenoliths along the Cheyenne belt and vicinity. *Rocky Mountain Geology*, *33*(2), 293–304. https://doi.org/10.2113/33.2.293

Li, Z.-X. A., Lee, C.-T. A., Peslier, A. H., Lenardic, A., & Mackwell, S. J. (2008). Water contents in mantle xenoliths from the Colorado Plateau and vicinity: Implications for the mantle rheology and hydration-induced thinning of continental lithosphere. *Journal of Geophysical Research*, *113*, B09210. https://doi.org/10.1029/2007JB005540

Lin, Y., Hui, H., Li, Y., Xu, Y., & Van Westrenen, W. (2019). A lunar hygrometer based on plagioclase-melt partitioning of water. *Geochemical Perspectives Letters*, *10*, 14–19.

McLelland, J. M., & Whitney, P. R. (1980). A generalized garnet-forming reaction for metaigneous rocks in the Adirondacks. *Contributions to Mineralogy and Petrology*, *72*(2), 111–122. https://doi.org/10.1007/BF00399472

Mosenfelder, J. L., Le Voyer, M., Rossman, G. R., Guan, Y., Bell, D. R., Asimow, P. D., & Eiler, J. M. (2011). Analysis of hydrogen in olivine by SIMS: Evaluation of standards and protocol. *American Mineralogist*, *96*(11–12), 1725–1741. https://doi.org/10.2138/am.2011.3810

Mosenfelder, J. L., & Rossman, G. R. (2013a). Analysis of hydrogen and fluorine in pyroxenes: I. Orthopyroxene. *American Mineralogist*, *98*(5-6), 1026–1041. https://doi.org/10.2138/am.2013.4291

Mosenfelder, J. L., & Rossman, G. R. (2013b). Analysis of hydrogen and fluorine in pyroxenes: II. Clinopyroxene. *American Mineralogist*, *98*(5–6), 1042–1054. https://doi.org/10.2138/am.2013.4413

Muntener, O., & Ulmer, P. (2006). Experimentally derived high-pressure cumulates from hydrous arc magmas and consequences for the seismic velocity structure of lower arc crust. *Geophysical Research Letters*, *33*, L21308. https://doi.org/10.1029/2006GL027629

Paterson, S. R., Fowler, T. K. Jr., Schmidt, K. L., Yoshinobu, A. S., Yuan, E. S., & Miller, R. B. (1998). Interpreting magmatic fabric patterns in plutons. *Lithos*, *44*(1–2), 53–82. https://doi.org/10.1016/S0024-4937(98)00022-X

Plank, T., Kelley, K. A., Zimmer, M. M., Hauri, E. H., & Wallace, P. J. (2013). Why do mafic arc magmas contain ~4wt% water on average? *Earth and Planetary Science Letters*, *364*, 168–179. https://doi.org/10.1016/j.epsl.2012.11.044

Plank, T., & Langmuir, C. H. (1988). An evaluation of the global variations in the major element chemistry of arc basalts. *Earth and Planetary Science Letters*, *90*(4), 349–370. https://doi.org/10.1016/0012-821X(88)90135-5

Rapp, R. P., Shimizu, N., & Norman, M. D. (2003). Growth of early continental crust by partial melting of eclogite. *Nature*, *425*(6958), 605–609. https://doi.org/10.1038/nature02031

Reid, A. M., Donaldson, C. H., Brown, R. W., Ridley, W. I., & Dawson, J. B. (1975). 36 - Mineral chemistry of peridotite xenoliths from the Lashaine volcano, Tanzania. In L. H. Ahrens, et al. (Ed.), *Physics and chemistry of the Earth* (pp. 525–543). Elsevier. https://doi.org/10.1016/B978-0-08-018017-5.50040-7

Saltzer, R. L., Chatterjee, N., & Grove, T. L. (2001). The spatial distribution of garnets and pyroxenes in mantle peridotites: Pressure-temperature history of peridotites from the Kaapvaal Craton. *Journal of Petrology*, *42*(12), 2215–2229. https://doi.org/10.1093/petrology/42.12.2215

Scholl, D. W., Vallier, T. L., & Stevenson, A. J. (1986). Terrane accretion, production, and continental growth: A perspective based on the origin and tectonic fate of the Aleutian–Bering Sea region. *Geology*, *14*(1), 43–47. https://doi.org/10.1130/0091-7613(1986)14<43:TAPACG>2.0.CO;2

Sobolev, A. V., & Chaussidon, M. (1996). H_2O concentrations in primary melts from supra-subduction zones and mid-ocean ridges: Implications for H_2O storage and recycling in the mantle. *Earth and Planetary Science Letters*, *137*(1–4), 45–55. https://doi.org/10.1016/0012-821X(95)00203-O

Tenner, T. J., Hirschmann, M. M., Withers, A. C., & Hervig, R. L. (2009). Hydrogen partitioning between nominally anhydrous upper mantle minerals and melt between 3 and 5 GPa and applications to hydrous peridotite partial melting. *Chemical Geology*, *262*(1-2), 42–56. https://doi.org/10.1016/j.chemgeo.2008.12.006

Whitmeyer, S. J., & Karlstrom, K. E. (2007). Tectonic model for the Proterozoic growth of North America. *Geosphere*, *3*(4), 220–259. https://doi.org/10.1130/GES00055.1

Yang, X. Z., Deloule, E., Xia, Q. K., Fan, Q. C., & Feng, M. (2008). Water contrast between Precambrian and Phanerozoic continental lower crust in eastern China. *Journal of Geophysical Research*, *113*, B08207. https://doi.org/10.1029/2007JB005541

Zhao, Y.-H., Ginsberg, S., & Kohlstedt, D. (2004). Solubility of hydrogen in olivine: Dependence on temperature and iron content. *Contributions to Mineralogy and Petrology*, *147*(2), 155–161. https://doi.org/10.1007/s00410-003-0524-4